Online Adaptive Model Identification and State of Charge Estimation for Vehicle-Level Battery Packs

Xiaohua Wu, Junhao Shu, Zhanfeng Fan, Jianbo Xie, Yang Li, *Senior Member, IEEE*, Jibin Yang, and Zhongwei Deng, *Member, IEEE*

***Abstract*—Accurate state of charge (SOC) estimation of traction batteries plays a crucial role in energy and safety management for electric vehicles. Existing studies focus primarily on cell battery SOC estimation. However, numerical instability and divergence problems might occur for a large-size lithium-ion battery pack consisting of many cells. This paper proposes a high-performance online model identification and SOC estimation method based on an adaptive square root unscented Kalman filter (ASRUKF) and an improved forgetting factor recursive least squares (IFFRLS) for vehicle-level traction battery packs. The model parameters are identified online through the IFFRLS, where the conventional method might encounter numerical stability problems. By updating the square root of the covariance matrix, the divergence problem in the traditional unscented Kalman filter is solved in the ASRUKF algorithm, where the positive semi-definiteness of the covariance matrix is guaranteed. Combined with the adaptive noise covariance matched filtering algorithm and real-time compensation of system error, the proposed method solves the problem of ever-degrading estimation accuracy in the presence of time-varying noise with unknown statistical characteristics. Using a 66.2-kWh vehicle battery pack, we experimentally verified that the proposed algorithm could achieve high estimation accuracy with guaranteed numerical stability. The maximum error of SOC estimation can be bounded by 1%, and the root-mean-square error is as low as 0.47% under real-world vehicle operating conditions.**

***Index Terms*—State of charge, Equivalent circuit model, Adaptive square root unscented Kalman filter, Forgetting factor recursive least squares**

I. Introduction

THE global automotive industry is rapidly transitioning towards cleaner and more efficient electric vehicles (EVs) [1]. Traction lithium-ion batteries have become a significant research and application area in the field of new energy vehicles due to their high specific energy, small size, and good recyclability. However, the level of the available energy stored in the battery cannot be measured directly. It can only be estimated based on limited external measurements such as voltage, current, and surface temperature. Due to lithium-ion batteries' high-dimensional and nonlinear characteristics, accurate state of charge (SOC) estimation needs to be revised. It is considered one of the main problems limiting EV development. Therefore, developing a battery SOC estimation algorithm with high accuracy and strong robustness for real-time operation is challenging and highly rewarding. [2], [3].

Proper modeling and accurate parameter estimation are essential to ensure traction batteries' efficient and reliable operation. The existing battery models mainly include the electrochemical model [4], [5], the equivalent circuit model (ECM) [6], and the data-driven model [7]. Many scholars have analyzed the characteristics of these three types of models. Although the electrochemical models are promising for future advanced battery management, they are complex and computationally intensive and not feasible for low-cost applications at the current stage [8]. Data-driven methods require a large amount of experimental data to train the model if acceptable prediction accuracy needs to be achieved [9]. To characterize the external properties of traction batteries, the ECM uses circuit elements such as resistors, capacitors, and voltage sources to form a circuit network. The ECMs are preferred by most industrial applications owing to their simple parameter identification, low computational burden, high real-time performance, and precision [10]. ECMs include the Rint model, the RC model, the Thevenin model, the PNGV model, and fractional-order models [11]. Among them, the first-order RC ECM is mainly adopted in the literature because of its low algorithm complexity and simple hardware implementation.

Parameter identification can be divided into offline and online techniques. Offline methods are to find a mapping from measurements to parameters, which can be obtained by using standard testing profiles (e.g., hybrid pulse power characteristics test [12]) or electrochemical impedance spectroscopy [13]. However, since battery parameters are affected by many factors, for instance, SOC, temperature, current rate, current frequency, and aging, obtaining a comprehensive relationship describing the parameter relationship requires excessive test time. In contrast, online methods use real-time measurements to update battery model parameters. The leading online algorithms include particle swarm optimization

This work was supported in part by Science and Technology Department of Sichuan Province (Grant Nos. 2023YFG0067, 2020YFQ0037, 2021YFG0071, 2021YFQ0052), Xihua University Fund (Grant No. QCCK2022-001), Open Fund of Sichuan Engineering Research Center for Mechanical Properties and Engineering Technology of Unsaturated Soils (Grant No. SC-FBHT2022-14), China Scholarship Council (CSC No. 202105530027). *(Corresponding authors: Xiaohua Wu and Zhanfeng Fan)*

X. Wu, J. Shu, and J. Yang are with Vehicle Measurement Control and Safety Key Laboratory of Sichuan Province, School of Automobile and Transportation, Xihua University, Chengdu, 610039, China. (e-mails: xiaohuawu13@163.com; 1356655853@qq.com; yangjibin08@163.com).

Z. Fan is with Sichuan Engineering Research Center for Mechanical Properties and Engineering Technology of Unsaturated Soils, School of Architecture and Civil Engineering, Chengdu University, Chengdu, 610106, China. (e-mail: fzhf213@163.com).

J. Xie is with WM Motor Technology Group Company Limited, Chengdu, 610101, China. (e-mail: 2249325257@qq.com).

Y. Li is with Department of Electrical Engineering, Chalmers University of Technology, Gothenburg, 41296, Sweden. (e-mail: yangli@ieee.org).

Z. Deng is with School of Mechanical and Electrical Engineering, University of Electronic Science and Technology of China, Chengdu, 611731, China. (e-mail: dengzw1127@gmail.com).

(PSO) [14], Kalman filter (KF) [15], and recursive least squares (RLS) [16]. The RLS is widely used for parameter identification, where the measurement data at the current time instant is used to modify the parameters computed at the previous time instant. Therefore, the RLS has the advantages of simple operation and low computation and is suitable for the online process [17]. However, due to the accumulation of information from historical data, the recursive results of the standard RLS cannot focus on the features in new data. Therefore, the forgetting factor RLS (FFRLS) was proposed in [18]. The impacts of historical and contemporary data can be adequately balanced by introducing the forgetting element. The standard RLS and FFRLS are designed under relatively short-time, Gaussian data. In [19], an adaptive FFRLS was proposed to address long historical data with non-Gaussian white noise by introducing an adaptive forgetting factor and an augmented method. It should be noted that the above-mentioned online parameter identification algorithms require exact information on the initial state and covariance of the battery model to maintain sufficient numerical stability and accuracy. Furthermore, numerical stability and convergence are usually shown to be guaranteed under mildly frequent variations in the current excitation, which is less experienced in a modern EV system.

Indeed, assuming a suitable battery model and accurate parameters are available, many battery state estimation methods have shown their effectiveness under certain conditions. For example, there are plenty of SOC estimation methods proposed in the literature, including the Coulomb counting method, the open-circuit voltage (OCV) method, data-driven methods, and model-based methods. The Coulomb counting method is a simple open-loop method, but it can cause SOC cumulative error owing to inaccurate initial SOC or the current measurement error [20]. In the OCV method, the relationship between OCV and SOC can be obtained with a fixed discharge rate, from which the corresponding SOC for a given OCV can be found. A programmable logic controller combining the Coulomb counting method and the OCV was proposed to manage lithium-ion batteries accurately in [21]. However, this method is susceptible to cell inconsistency, temperature variation, and aging [22], thus unsuitable for high-performance EV applications.

The rapid development of big data technologies has spawned many data-driven machine learning algorithms for battery SOC estimation in recent years [23]. This method describes the nonlinear relationship of battery variables with general mathematical models without the need to understand complex electrochemical mechanisms. Therefore, it has the advantages of high prediction accuracy, good numerical stability, and high adaptability. At present, the data-driven SOC estimation methods are mainly designed based on the long short-term memory neural network [24], deep neural network [25], Gaussian process regression [26], support vector machine [27], and so on. However, enough data storage space and complex and time-consuming calculations limit its promotion and application on battery management systems (BMSs).

The model-based method with a closed-loop feedback structure has the advantages of high estimation accuracy, low computational requirements, and easy implementation. Model-based methods include KF, sliding mode observer [28], [29], H-infinity filter [30], and other non-linear observers. The classical KF algorithm can accurately estimate the system state of a linear system by filtering out the interference of system errors and reducing the influence of measurement errors, where the errors are assumed to be Gaussian distributed. Since a battery system is nonlinear with a complex and ever-changing operating environment, researchers have proposed many improved KF algorithms to improve the state estimation accuracy [31]. For example, the extended KF (EKF) is superior to the Coulomb counting method in terms of accuracy and robustness [20]. However, the accuracy of the EKF is limited for a highly nonlinear system because it uses the Taylor series expansion to transform the nonlinear system into a linear system.

Furthermore, calculation of the Jacobian matrix is complicated and computational inefficient. Hence, various alternatives have been proposed, such as the central difference KF (CDKF) [32], cubature KF (CKF) [33], square root cubature KF (SRCKF) [34], unscented KF (UKF) [35], ensemble Kalman filter (EnKF) [36], etc. The UKF introduces the concept of unscented transformation (UT) that propagates a series of sigma points to calculate the state and the error covariance matrix, which track the statistics of a random variable when imported into a nonlinear function linearization process [37]. Although it solves the problem in the EKF caused by the linearization process, the UKF requires the state variables' covariance matrix to be positive and definite. Otherwise, the filtering algorithm may not converge. This positive definiteness is not guaranteed in the UKF, leading to possible numerical problems. The square-root UKF (SRUKF) uses the square root of the state variable covariance matrix to replace the covariance in the UKF, and it avoids the filter divergence problem caused by the non-positive definiteness of the covariance matrix [38]. However, in the above algorithms, the system and measurement noise covariance matrices are usually assumed to be constant. The inaccurate noise statistical information can also lead to filter divergence. Therefore, the Sage-Husa adaptive filtering uses the innovation and residual sequence between the measured and the predicted values to revise the estimated system noise covariance. The estimation divergence caused by inaccurate noise can be avoided [39].

Currently, the FFRLS and KF-based algorithms have been widely used in the SOC estimation of traction batteries, and the algorithm has good accuracy through the cell test. However, we find that many standard algorithms have problems in practical applications, mainly because of the following reasons. First, the actual operating conditions of the BMS are more complex, and the acquisition conditions are more severe. Therefore, it is prone to abnormal identification of model parameters, such as negative resistance and imaginary number. Second, the ECM is always preferred for practical systems. Still, it is oversimplified for describing the complex dynamic behavior of a large battery pack that consists of many cells, which can directly cause the divergence of the KF and RLS algorithms. Furthermore, the convergence speed and estimation accuracy of the KF algorithm is significantly affected

by the algorithm's parameters, such as the error covariance matrix, process noise covariance matrix, measurement noise covariance matrix, and their initial values. At the same time, their tuning is usually based on unreliable initial trial and error. We will discuss these problems in the latter sections.

This work establishes a vehicle-level battery SOC estimation framework that consists of adaptive SRUKF and improved FFRLS (IFFRLS-ASRUKF), static calibration strategy, full-charge calibration strategy, and operating condition discrimination modules to overcome the shortcomings of the studies mentioned above. Furthermore, this SOC estimation framework mitigates the impact of uncertain initialization parameters, such as the initial SOC, process noise covariance, and measurement noise covariance, on the estimation accuracy, leading to enhanced numerical stability and convergence speed. The main novelties and contributions of this work include the followings.

First, we propose an improved FFRLS algorithm where an adaptive forgetting factor and a sliding time window with a fuzzy threshold are integrated, denoted by IFFRLS. The IFFRLS solves the problem caused by abnormal parameters estimate during online identification using conventional FFRLS. It also improves the algorithmic accuracy and stability for real-time operation.

Second, two online calibration strategies are proposed for practical operation. The static calibration strategy is mainly aimed at the initial SOC calibration when the battery is powered on, and the full-charge calibration strategy is primarily aimed at the charging. These calibration strategies not only improve the convergence speed and accuracy of the algorithm but also optimize the negative impact of incorrect initial parameters on the accuracy of the algorithm.

Third, we notice that low-rate constant current discharge conditions during practical vehicle operation could easily lead to a drift in online parameter identification, causing an increased error when an RLS-based algorithm is adopted. A working condition discrimination module for such complex operating conditions is therefore established by switching between the Coulomb counting method and the proposed IFFRLS–ASRUKF algorithm.

II. Online parameter identification

A. Battery Pack Model

The ECM is a circuit network composed of resistance, capacitance, constant voltage source and other circuit components to describe the external characteristics of the battery. The schematic of the ECM of n-order RC is shown in Fig. 1. Where U_{oc} is the OCV which has a nonlinear relationship with temperature and SOC. R_0 and R_n are the ohmic and the electrochemical polarization resistances, respectively. C_n is the electrochemical capacitance. I is the operating current, defined as positive during discharge. U_t is the terminal voltage of the battery. U_n represents the polarization voltage. Where $n = 0$ is the Rint model, $n = 1$ is the first-order RC equivalent circuit model, and $n = 2$ is the second-order RC equivalent circuit model.

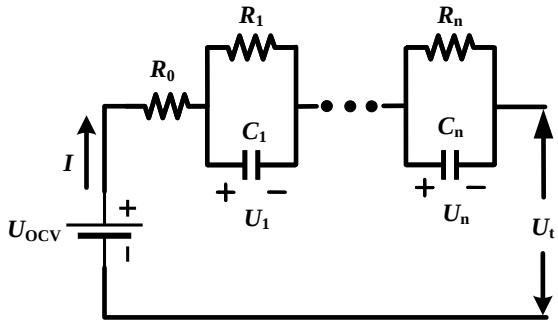

Fig. 1. ECM of n-order RC.

In order to balance the complexity and accuracy of the model, the number of RC parallel needs to be selected according to the actual situation. The Rint model cannot accurately predict the characteristics of the battery under dynamic operating conditions. The calculation accuracy may increase with the increase of the number of RC parallel structures, but at the expense of higher model complexity and computational load. In this work, a first-order RC model of the battery is adopted because of its simplicity and easy implementation, i.e. [40],

$$\begin{cases} \dot{U}_1 = -\frac{1}{C_1 R_1} U_1 + \frac{1}{C_1} I \\ U_t = U_{oc} - U_1 - I R_0 \end{cases} \tag{1}$$

Next, the SOC of the battery is defined as the ratio of the remaining available capacity to the present true capacity C of the battery [41], and it can be modeled using the Coulomb counting:

$$\begin{cases} \dot{SOC} = -\frac{\eta I}{C} \\ C = SOH \times C_0 \end{cases} \tag{2}$$

where η is the Coulombic efficiency, SOH is state of health, C_0 is nominal capacity.

After discretizing the model with a sampling time of Δt, (1) and (2) can be expressed in the discrete-time domain as [42],

$$\begin{pmatrix} U_{1,k+1} \\ SOC_{k+1} \end{pmatrix} = \begin{pmatrix} \exp(-\frac{\Delta t}{C_1 R_1}) & 0 \\ 0 & 1 \end{pmatrix} \times \begin{pmatrix} U_{1,k} \\ SOC_k \end{pmatrix} + \begin{pmatrix} R_1(1 - \exp(-\frac{\Delta t}{C_1 R_1})) \\ -\frac{\eta \Delta t}{C} \end{pmatrix} I_k \tag{3}$$

$$U_{t,k} = U_{oc,k} - U_{1,k} - I_k R_0 \tag{4}$$

B. Improved FFRLS

In (3) and (4), the parameters R_0, R_1, and C_1 can change with temperature, current, SOC, and battery aging. Offline parameterization might require extensive experimental studies and result in high-dimensional look-up tables. Instead, we use online identification based on the FFRLS with the sliding time window to update these parameters in real-time.

First, we apply the Laplace transform to (1), yielding

$$U_{oc}(s) - U_t(s) = I(s)(R_0 + \frac{R_1}{1 + R_1 C_1 s}) \tag{5}$$

Thus, the system transfer function is expressed as,

$$G(s) = \frac{U_{oc}(s) - U_t(s)}{I(s)} = \frac{R_0 + R_1 + R_0 R_1 C_1 s}{1 + R_1 C_1 s} \tag{6}$$

The bilinear transformation is used here to convert (6) from the s plane to the z plane. Specifically, letting $s = \frac{2}{\Delta t}\frac{1-z^{-1}}{1+z^{-1}}$, (6) becomes

$$G(z^{-1}) = \frac{a_2 + a_3 z^{-1}}{1 + a_1 z^{-1}} \tag{7}$$

where

$$\begin{cases} a_1 = \frac{\Delta t - 2R_1C_1}{\Delta t + 2R_1C_1} \\ a_2 = \frac{R_0\Delta t + R_1\Delta t + 2R_0R_1C_1)}{\Delta t + 2R_1C_1} \\ a_3 = \frac{R_0\Delta t + R_1\Delta t - 2R_0R_1C_1)}{\Delta t + 2R_1C_1} \end{cases} \tag{8}$$

Further, the discretized form of (4) can be obtained by applying the inverse z-transformation of (7), i.e.,

$$y_k = \phi_k \theta_k + e_{Ls,k} \tag{9}$$

where

$$\begin{cases} y_k = U_{oc,k} - U_{t,k} \\ \phi_k = [y_{k-1}, I_k, I_{k-1}] \\ \theta_k = [a_1, a_2, a_3]^T \end{cases} \tag{10}$$

According to the FFRLS, the battery model parameter can be identified by [43]:

$$\begin{cases} K_k = P_{k-1}\phi_k^T(\lambda_{k-1} + \phi_k P_{k-1}\phi_k^T)^{-1} \\ \hat{\theta}_k = \hat{\theta}_{k-1} + K_k(y_k - \phi_k\hat{\theta}_{k-1}) \\ P_k = (P_{k-1} - K_k\phi_k P_{k-1})/\lambda_{k-1} \end{cases} \tag{11}$$

where $K_{Ls,k}$ is the gain vector, $\hat{\theta}_k$ stands for the estimated parameter, and $P_{Ls,k}$ indicates the covariance matrix. Furthermore, $\lambda \in [0.95, 1.0]$ shows the forgetting factor constant [44]. However, a constant forgetting factor cannot balance the stability and fast convergence of the algorithm. Therefore, to improve the performance of the FFRLS, an adaptive formula is introduced to change λ with the voltage prediction error adaptively.

$$\begin{cases} \varepsilon_k = round(((y_k - \phi_k\hat{\theta}_{k-1})/e_{base})^2) \\ \lambda_k = \lambda_{\min} - (1 - \lambda_{\min})h^{\varepsilon_k} \end{cases} \tag{12}$$

where e_{base} is the benchmark error, $round(n)$ denotes the integer closest to n, and $\lambda_{\min}$ is the minimum value set in the value range. Furthermore, $h \in [0, 1]$ is the sensitivity coefficient, which represents the sensitivity of the adaptive change effect of λ on the prediction error.

According to (8), the model parameters R_0, R_1, and C_1 can be calculated by

$$\begin{cases} R_0 = \frac{a_3 - a_2}{1 + a_1} \\ R_1 = \frac{2(a_1a_2 - a_3)}{a_1^2 - 1} \\ C_1 = \frac{\Delta t(a_1 - 1)^2}{4(a_3 - a_1a_2)} \end{cases} \tag{13}$$

Note that in (13), the standard FFRLS requires a reasonable guess of initial $\hat{\theta}_k$ and $P_{Ls,k}$, denoted by $\hat{\theta}_0$ and $P_{Ls,0}$, respectively. These initial values might require reliable prior knowledge of battery characteristics. In practice, many trial-and-error tests are needed for vehicle-level battery packs, and the results are difficult to be transferred to a different battery pack design. Furthermore, provided incorrect initial parameters and covariance are selected, the standard FFRLS might lead to numerical problems, e.g., slow convergence and even divergence.

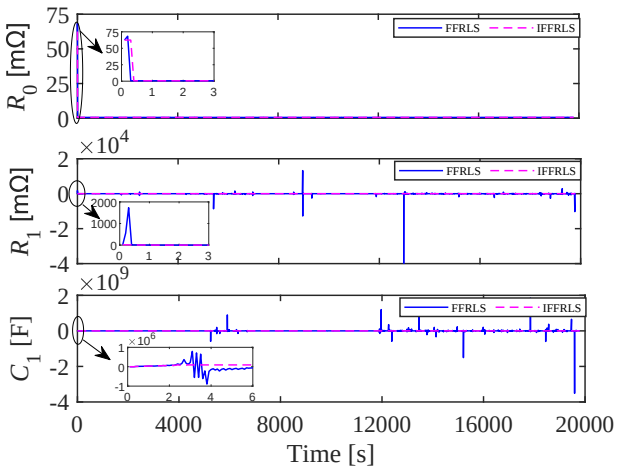

Fig. 2. Parameter identification results of FFRLS and IFFRLS under DST condition.

Therefore, an improved and simple-to-implement FFRLS algorithm with a sliding window (IFFRLS) is proposed. Taking the identified ohmic resistance as an example, the identification methods of the electrochemical polarization resistance and the electrochemical polarization capacitance are the same, and the way is given as follows,

$$R_{0,k} = \begin{cases} R_{0,k} & R_{0,k} \le R_{0\_limit} \\ \frac{1}{m}\sum_{i=k-m+1}^{k} R_{0,i} & R_{0,k} > R_{0\_limit} \end{cases} \tag{14}$$

where R_{0_limit} is the fuzzy threshold obtained by trial and error, $R_{0,i}$ is the ohmic resistance identified through the FFRLS, and m is the horizon of the sliding window.

The parameter identification results by comparing the IFFRLS with the FFRLS are shown in Fig. 2. The battery data comes from battery cell experiment as described in Section IV-A. It can be seen that parameters identified by the FFRLS can become negative and/or present abnormally high magnitude, which loses the physical meaning and lead to degraded prediction accuracy, and eventually divergence. Moreover, the parameter identification process based on the IFFRLS is stable after 60 time steps. In contrast, for the FFRLS, the process shows a high level of fluctuation. The results show that the IFFRLS converges faster than the FFRLS, and it ensures the parameters vary within reasonable ranges. This improves the dynamic performance as well as the numerical stability of the system.

III. A Framework of Battery Pack SOC Estimation

A. Adaptive Square Root Unscented Kalman Filter

This section proposes an adaptive square root unscented Kalman filter (ASRUKF). The ASRUKF mainly includes initialization, acquisition of sigma points, time update, QR decomposition, measurement, calculation of Kalman gain,

noise update, and other steps. It can ensure the semi-positive definiteness of the covariance matrix, prevent divergence during filtering, and enhance the algorithm's stability [45]. The adaptive covariance matching filtering algorithm can efficiently consider noise characteristics and improve the anti-interference ability of the algorithm. The basic steps of the ASRUKF are given in Table I, where the battery pack (3) and (4) is represented as a nonlinear stochastic discrete-time system [46]:

$$\begin{cases} x_k = f(x_{k-1}, u_{k-1}) + \omega_{k-1} \\ z_k = h(x_k, u_k) + v_k \end{cases} \tag{15}$$

Here, $x = [U_1, SOC]^T$ is the state vector, $u = I$ is the single input, and $z = U_t$ is the single measurable output. f and h are two functions for the state and output equations, respectively. Furthermore, ω and v are zero-mean Gaussian white noises, and the corresponding covariance metrics are Q and R, respectively.

Compared to the standard SRUKF with predefined and fixed error covariance matrices, a simple adaptive noise covariance matching filtering algorithm is introduced. The covariance of the system process error and the measurement error are updated online based on newly measured and estimated voltage sequences. It replaces the constant noise equation with the time-varying noise covariance closer to the actual operating state of the traction battery, thereby further improving the estimation accuracy. The adaptive noise covariance matching filter updates Q_k and R_k as follows [48]:

$$\begin{cases} e_k = z_k - \hat{z}_{k|k-1} \\ C_k = \frac{1}{l} \sum\limits_{i=k-l+1}^{l} e_i e_i^T \\ Q_k = K_k C_k K_k^T \\ R_k = C_k + \sum\limits_{i=1}^{2n} w_c^i (z_{k|k-1}^i - z_k)(z_{k|k-1}^i - z_k)^T \end{cases} \tag{16}$$

where e_k is the observation residual, C_k is the residual observation covariance, and l is a receding horizon.

B. Static Calibration Strategy

The static calibration strategy is triggered shortly after the battery is powered on. The specific trigger conditions include no abnormality in current, voltage and probe temperature acquisition, and the current is less than 0.01C, power on time is less than 30 seconds and no full charge calibration sign bit when the battery is powered down. If the static calibration conditions are met, the OCV correction method can be used for calibration according to the dormancy time. Furthermore, the OCV correction method can update the initial SOC through the OCV-SOC-Temp relationship. If the dormancy time is less than two hours, the OCV correction method and the Coulomb counting method will be used to correct the initial SOC, and the way is given in (17). Therefore, the specific algorithm logic for the static correction policy is shown in Fig. 3(a).

$$\begin{cases} SOC_0 = f(Temp, V), Time \geq 2h \\ SOC_0 = \frac{Time}{2h} f(Temp, V) + (1 - \frac{Time}{2h}) SOC_{Ah}, otherwise \end{cases} \tag{17}$$

TABLE I
BASIC STEPS OF THE ASRUKF.

Step 1 Initialization: the state estimate $\hat{x}_0$, the state estimation error covariance P_0 and the matrices Q and R.

$$\begin{cases} \hat{x}_0 = E(x_0) \\ S_0 = chol(P_0) \\ Q = Q_0 \\ R = R_0 \end{cases}$$

where, S_0 is Cholesky factor of P_0.

Step 2 Acquisition of the Sigma sampling points, the mean weight ω_m and the variance weight ω_c [39].

$$\begin{cases} x_{k-1}^i = \hat{x}_{k-1}, i = 0 \\ x_{k-1}^i = \hat{x}_{k-1} + (\sqrt{(n+\lambda)P_{k-1}})^i, i = 1, \ldots, n \\ x_{k-1}^i = \hat{x}_{k-1} - (\sqrt{(n+\lambda)P_{k-1}})^i, i = n+1, \ldots, 2n \end{cases}$$

$$\begin{cases} \omega_m^0 = \frac{\lambda}{n+\lambda} \\ \omega_c^0 = \frac{\lambda}{n+\lambda} + (1 + \alpha^2 + \beta) \\ \omega_m^i = \omega_c^i = \frac{1}{2(n+\lambda)}, i = 1, \ldots, 2n \end{cases}$$

Step 3 State variable time update.

$$\begin{cases} x_{k|k-1}^i = f(x_{k-1|k-1}^i, u_{k-1}) + \omega_{k-1}, i = 0, \ldots, 2n \\ \hat{x}_{k|k-1} = \sum\limits_{i=0}^{2n} \omega_m^i x_{k|k-1}^i \\ S_{x,k}^- = qr\{[\prod\limits_{i=1}^{2n} \sqrt{w_c^i}(x_{k|k-1}^i - \hat{x}_{k|k-1} \quad \sqrt{Q_{k-1}}\ ]^T\} \\ S_{x,k} = cholupdate\{S_{x,k}^-, x_{k|k-1}^0 - \hat{x}_{k|k-1}, w_c^0\} \end{cases}$$

where $qr(\cdot)$ is the QR decomposition and $cholupdate(\cdot)$ is the rank 1 update of the Cholesky decomposition.

Step 4 Observation updating [47].

$$\begin{cases} \xi_{k-1} = [\hat{x}_{k|k-1}, \hat{x}_{k|k-1} + \sqrt{n+\lambda} S_{x,k}, \hat{x}_{k|k-1} - \sqrt{n+\lambda} S_{x,k}] \\ z_{k|k-1}^i = h(\xi_{k-1}, u_k) \\ \hat{z}_{k|k-1} = \sum\limits_{i=0}^{2n} \omega_m^i z_{k|k-1}^i \\ S_{z,k}^- = qr\{[\prod\limits_{i=1}^{2n} \sqrt{w_c^i}(z_{k|k-1}^i - \hat{z}_{k|k-1}) \quad \sqrt{R_{k-1}}\ ]^T\} \\ S_{z,k} = cholupdate\{S_{z,k}^-, z_{k|k-1}^0 - \hat{z}_{k|k-1}, w_c^0\} \end{cases}$$

Step 5 Calculate the joint covariance matrix of the state variable $P_{xz,k}$ and the output variable at the moment k.

$$P_{xz,k} = \sum_{i=0}^{2n} \omega_c^i (x_{k|k-1}^i - \hat{\hat{x}}_{k|k-1})(z_{k|k-1}^i - \hat{\hat{z}}_{k|k-1})^T$$

Step 6 Calculate the Kalman gain K_k.

$$K_k = (P_{xz,k}/S_{z,k}^T)/S_{z,k}$$

Step 7 Update the Cholesky factor for the estimated value and the optimal covariance.

$$\begin{cases} \hat{x}_k = \hat{x}_{k|k-1} + K_k(z_k - \hat{z}_{k|k-1}) \\ S_k = cholupdate\{S_{x,k}, K_k S_{z,k}, -1\} \end{cases}$$

Step 8 Noise estimation. See Eq.(16).

where SOC_0 is the corrected initial SOC, $f(Temp, V)$ is the OCV-SOC-Temp relationship function, SOC_{Ah} is the calculated SOC by the Coulomb counting method.

C. Full-charge Calibration Strategy

The inconsistency of the traction battery cells is unavoidable. During the charging process, the estimated SOC of the maximum voltage cell is equivalent to the power battery SOC, which can effectively avoid overcharging and reflect the accurate SOC of the traction battery pack. The full-charge correction conditions for the traction battery are: 1) The maximum cell voltage reaches the limited charge voltage, and the terminal current is less than 0.23C under the fast charging mode or 0.06C under the slow charging mode for

20 s. 2) The total voltage reaches the limited charge voltage for 10 s. Then, the SOC is corrected to 100% when getting the complete charge condition. The algorithm logic of the full-charge calibration policy is shown in Fig. 3(b).

D. Operating Condition Discrimination Module

The operating conditions of traction battery packs are very complex. It can be roughly divided into low current constant current condition, dynamic low current condition, high constant current condition, and dynamic high current condition, taking charge and discharge current as the distinguishing mark. Through the verification of the test data, the low constant current discharge and charge condition can easily lead to the online parameter identification drift, which will inevitably degrade the accuracy of the designed model-based SOC estimator. Therefore, this paper proposes to establish a working condition discrimination module. First, a time window (e.g., 10 s) is set. If the sample mean (SM) and root mean square error (RMSE) are both lower than the threshold value, SM and RMSE values can be expressed in (18), and the window is judged as a minor current constant current condition. Then, under low current and constant current conditions, the SOC is estimated directly by the Coulomb counting method. Otherwise, the IFFRLS-ASRUKF algorithm is used. Therefore, when the sign bit is 0, 1, 2 and 3, the static correction, the Full-charge calibration, the Coulomb counting, and the IFFRLS is used, respectively. It can improve the SOC estimation accuracy and ensure algorithm stability. The principle of the operating condition discrimination module is shown in Fig. 3(c).

$$\begin{cases} \mathrm{SM} = \frac{1}{l}\sum_{j=k-l+1}^{k} x_j \\ \mathrm{RMSE} = \sqrt{\frac{1}{l}\sum_{j=k-l+1}^{k}\left(x_j - \mathrm{SM}\right)^2} \end{cases} \tag{18}$$

where l is the time window length, x_j is the current in the time window.

The battery data used are from the condition identification module in Section IV-B, and are identified at a low-rate constant current condition within the period from 6198.9 s to 8851.0 s. As can be seen from Fig. 4, this operating condition is prone to diverge under the FFRLS, leading to algorithm termination. With the IFFRLS, the identified resistance can be limited to a reasonable range, but it changes dynamically and tends to reach a constant value. This indicates that the IFFRLS can correct the outliers but fails to restore the normal identification results. It will lead to the reduction of the estimation accuracy of the terminal voltage and SOC. An algorithm error occurs. Therefore, in this operating condition, we propose to use the Coulomb counting method to estimate SOC to ensure the accuracy and numerical stability of the algorithm.

IV. Experimental Verification and Analysis

The overall framework of the proposed algorithms is summarized as shown in Fig. 5. In the light of Section II and Section III, the first-order RC model, IFFRLS, ASRUKF, the static calibration module, the full-charge calibration module, and the operating condition discrimination module were built

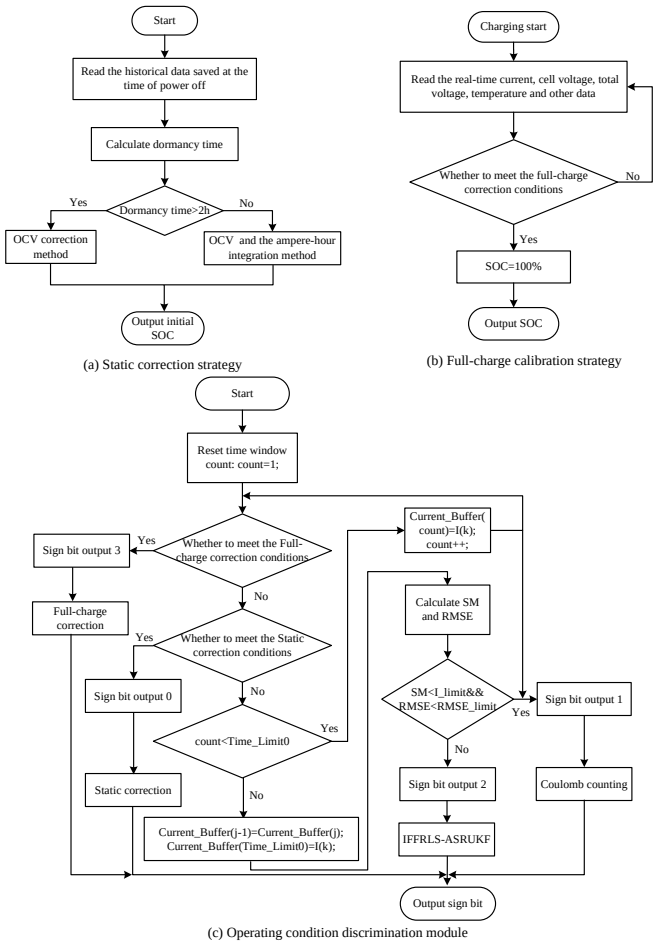

Fig. 3. Algorithm's logic flow charts. (a) Static correction strategy. (b) Full-charge calibration strategy. (c) Operating condition discrimination module.

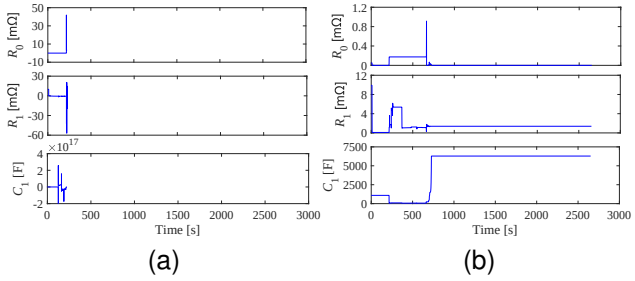

Fig. 4. Parameter identification results under a low-rate constant current condition based on (a) FFRLS and (b) IFFRLS.

and simulated in MATLAB. The battery OCV has a strong nonlinear relationship with the temperature and SOC of the traction battery. Thus it must be accurately reflected during the online operation of the ASRUKF. A 3D look-up table that describes the OCV-SOC-T relationship is established through the linear fitting. The input variables are the measured battery current, voltage, temperature, relay signal, and charge and discharge commands. The output variables are the estimated SOC, the estimated voltage, and the estimated model parameters. The horizon of the sliding window in the IFFRLS is

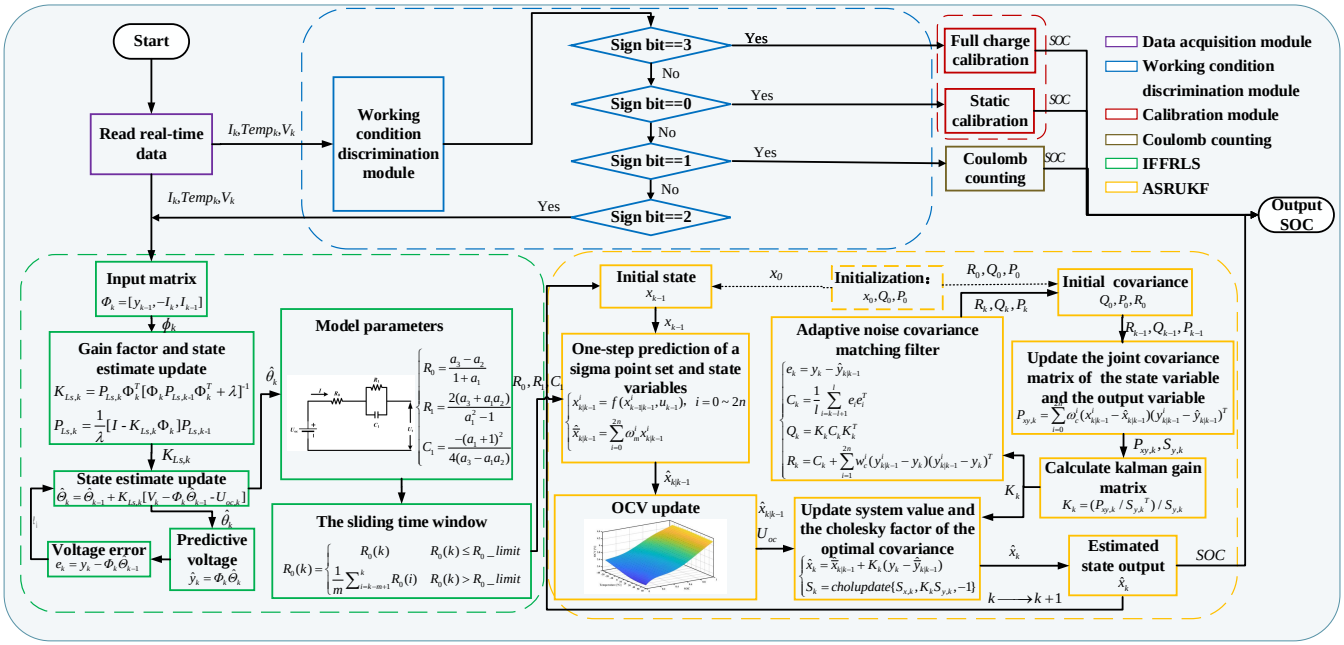

Fig. 5. Algorithmic framework for the proposed SOC estimation method for vehicle-level battery.

selected as $m = 60$ via trial and error.

A. Battery Cell Experiment

A platform was established to verify the proposed method based on a series of battery cell characteristic tests and cycle test experiments, as shown in Fig. 6. The experimental battery cell was $LiNi_xCo_yMn_zO_2$ (NCM) battery pack with a nominal capacity of 66.2-kWh. The test equipment was Chroma 69212 charge and discharge test cabinets, which could perform pulse charge and discharge tests, constant current charge and discharge tests, constant voltage charge-discharge tests, complex cycle condition tests, etc. The data were recorded, including voltage, current, charge-discharge capacity, temperature, and other data during the tests. The sampled rate was 100 ms. The SANWOOD's high and low-temperature experimental box provided a stable temperature environment.

The dynamic stress test (DST) condition is a standard operating condition for simulating EV urban driving according to USABC Electric Vehicle Battery Test Procedures Manual [49] and it was used to verify the accuracy of the algorithm. The identification results of the battery cell model parameters are shown in Fig. 7. It can be seen that the model parameters have been oscillated and revised as time increased, but they remain within a reasonable range. The errors of the model terminal voltage are shown in Fig. 8. The error between the model-predicted terminal voltage and the actual measured terminal voltage is less than 0.015 V, which has an accurate terminal voltage prediction accuracy.

The SOC estimation results under the DST condition with accurate/inaccurate initial SOC values are shown in Fig. 9. For comparison, we use the same online parameter identification method with different SOC estimation filtering algorithms of Adaptive EKF (AEKF) [19] and Adaptive UKF (AUKF) [50], and the corresponding algorithms are denoted by IFFRLS-AEKF and IFFRL-SAUKF, respectively. With accurate initial SOC value, Figs. 9(a) and (b) show the estimation SOC and error. The maximum error, mean absolute error (MAE), and RMSE for the three algorithms are shown in Table II. It can be seen that the maximum error, MAE, and RMSE of the IFFRLS-ASRUKF are only 0.23%, 0.14%, and 0.15%, respectively, which are better than the other two algorithms. With inaccurate initial SOC value, Figs. 9(c) and (d) show the estimation SOC and error. The MAE, RMSE and convergence time for the three algorithms are also shown in Table II. The MAE, RMSE, and convergence time of the IFFRLS-ASRUKF are 0.30%, 0.30%, and 11.2 s, respectively. The convergence time of the IFFRLS-ASRUKF is slightly higher than that of the IFFRLS-AEKF, but the MAE and RMSE of the IFFRLS-ASRUKF algorithm are better than the other two algorithms. Therefore, the IFFRLS-ASRUKF has high estimation accuracy and a fast convergence rate.

TABLE II
PERFORMANCE COMPARISON OF IFFRLS-BASED ADAPTIVE SOC ESTIMATION METHODS UNDER DST CONDITION WITH KNOWN/UNKNOWN INITIAL SOC

Method	Init. SOC	Max. Err.	MAE	RMSE	Conv. Time
ASRUKF	Known	0.23%	0.14%	0.15%	–
AEKF	Known	1.71%	0.40%	0.46%	–
AUKF	Known	0.32%	0.22%	0.22%	–
ASRUKF	Unknown	–	0.30%	0.30%	11.2 s
AEKF	Unknown	–	0.63%	0.68%	13.8 s
AUKF	Unknown	–	0.60%	0.61%	18.3 s

Initialization parameters significantly influence the accuracy

and convergence speed of model estimation. For example, with the accuracy and inaccuracy initial SOC, the same initial process noise covariance Q_0, and measurement noise covariance R_0 value, the estimation accuracy can not achieve the expected effect, as shown in Fig. 10. With the same $Q_0 = \text{diag}([0.0001, 0.0001])$, $R_0 = 0.1$, if the initial SOC is inaccurate, the accuracy of the model prediction method is very low. In the BMS, manually adjusting the initial parameters to deal with the inaccuracy in the initial SOC is impractical. Therefore, we propose a static and full calibration strategy to calibrate SOC value quickly and avoid the impact of incorrect initial parameters on SOC estimation.

B. Vehicle-level Battery Pack Experiment

For the problems mentioned above, a set of SOC estimation frameworks, including the IFFRLS-ASRUKF, static calibration strategy, full-charge calibration strategy, and operating condition discrimination module for the vehicle-level battery pack, is proposed to solve the impact of initial parameters on the estimation accuracy. In addition, a specific traction battery pack of an EV was selected as the experimental object to verify the state estimation effect of the algorithms for the vehicle-level battery pack. The basic parameters of the vehicle-level battery pack are shown in Table III.

TABLE III
SPECIFICATION OF THE BATTERY PACK

Parameter	Value	Unit
Cell type	NCM	–
Pack nominal capacity	177	Ah
Cell nominal voltage (1C)	3.66	V
Pack grouping method	3P104S	–
Pack nominal power (1C)	66.231	kWh
Charge termination voltage	4350	mV
Discharge termination voltage	2800	mV
Pack total voltage upper limit	450.84	V
Pack total voltage lower limit	219.20	V

The Kvaser device of Weber Electronics Co., Ltd. was adopted for actual vehicle data acquisition. It had high time stamp accuracy and efficiently processed the reception and

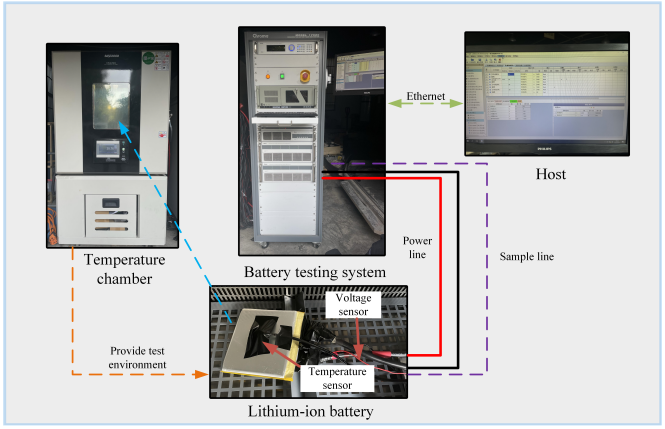

Fig. 6. Battery experimental platform.

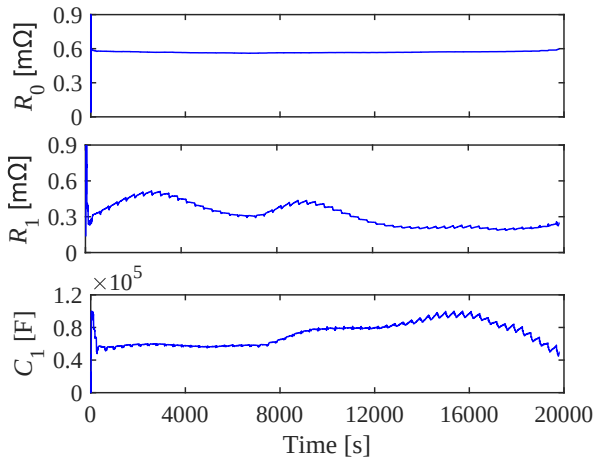

Fig. 7. Identified model parameters under the DST condition.

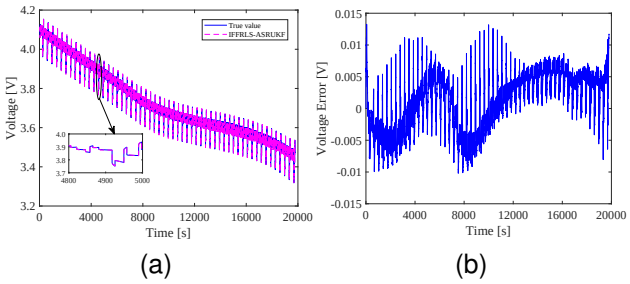

Fig. 8. Comparison of the measured and estimated battery voltage under the DST condition. (a) Estimated and measured voltages. (b) Voltage error.

transmission of standard and extended CAN messages. The data collection interval was 100 ms. The collected data included the vehicle speed, the bus current, the bus voltage, the temperature of each probe, the cell voltage, the charge and discharge signals, the high-voltage relay signals, etc.

Real-world EV operating data of one week, including six charge-discharge cycles, were used for evaluating the algorithm. The battery current, terminal voltage, temperature, and vehicle speed are shown in Fig. 11. Since the vehicle operating conditions are complex and random, the current of the traction battery changes drastically.

The identified vehicle-level battery pack model parameters are shown in Fig. 12(a). The vehicle-level battery pack model parameters are continuously revised during the identification process. Only when the sign bit is 2, the battery parameters are identified and updated online. In other sign bits, the parameters identified from the previous step will be adopted and thus the online update is not needed. It can be found that there are sudden abnormal increases or decreases in battery parameter data in Fig. 12(a). Fig. 12(b) shows that the time point corresponds to the static correction condition. This is because the initial battery temperature is very low. When the battery is powered on, the temperature gradually rises and is regulated within a designed high-temperature operating range with the assistance of thermal management. The temperature will affect many model parameters, such as the battery

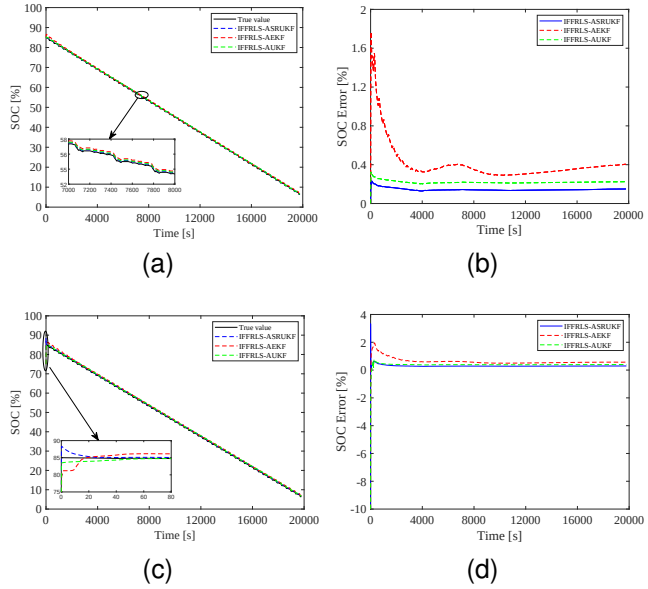

Fig. 9. Comparison of SOC estimation results using different algorithms under the DST condition. (a) SOC estimation with known initial value. (b) Estimation error with known initial value. (c) SOC estimation with unknown initial value. (d) Estimation error with unknown initial value.

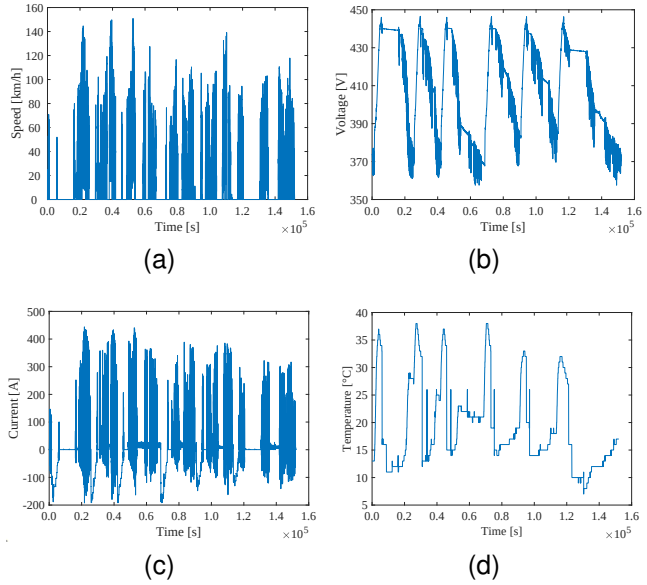

Fig. 11. Real-world EV operating data. (a) Vehicle speed. (b) Battery voltage. (c) Battery current. (d) Battery temperature.

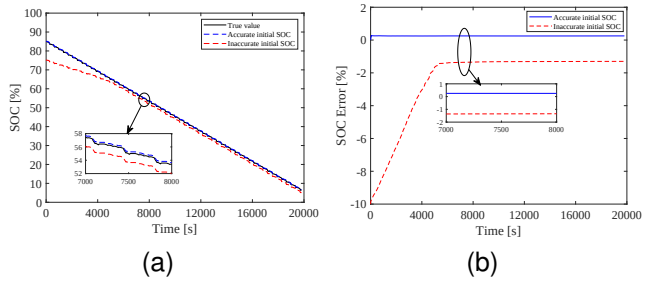

Fig. 10. Comparison of SOC estimation results with accurate/inaccurate initial SOC. (a) SOC estimation result. (b) SOC estimation error.

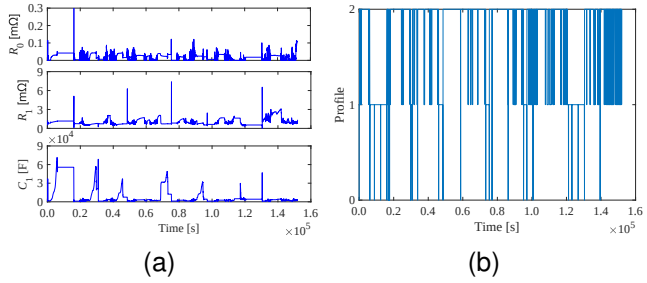

Fig. 12. Identified results under real-world EV operating data. (a) Identified model parameters. (b) Output of the working condition discrimination module.

capacity in the state equation, the OCV in the observation equation, as well as circuit parameters. Since the initial battery parameters were identified and stored in the previous running process where the temperature might be very different from the present, the accuracy of the model can be significantly reduced. Therefore, the parameter correction is prominent at this time. According to the predicted voltage error, the correct model parameters will be quickly calculated through continuous iteration. The working condition discrimination values are shown in Fig. 12(b). The working conditions that are difficult to identify can be accurately determined, improving the algorithm's convergence. For example, 1 is the time of the Coulomb counting, 2 is the time of the IFFRLS-ASRUKF, and 0 is the time of the static correction strategy.

The SOC estimation results of the vehicle-level battery pack are shown in Fig. 13 and the performance is summarized in Table IV. The algorithms under comparison are IFFRLS-AEKF and IFFRLS-AUKF, in which the AEKF and AUKF are used to replace the ASRUKF when SOC estimation. Due to the initial SOC's inaccuracy, the early SOC's error is significant for the IFFRLS-AEKF. With the continuous iteration of the algorithm, the maximum error of the corrected SOC for the IFFRLS-ASRUKF algorithm is 2.15%. And with constant correction and iteration, the maximum error is within 1%. The MAE and RMSE of the IFFRLS-ASRUKF are 0.22% and 0.47%, respectively. The maximum error of the SOC estimation of the IFFRLS-AEKF algorithm is within 3.74%, and the MAE and RMSE are 0.58% and 0.88%, respectively. The maximum error of the SOC estimation of the IFFRLS-AUKF algorithm is within 4.92%, and the MAE and RMSE are 0.42% and 0.79%, respectively. Compared with the IFFRLS-AEKF and the IFFRLS-AUKF, the IFFRLS-ASRUKF significantly improves the estimation accuracy, fitting speed, and SOC stability. And when the initial SOC is inaccurate, the convergence rate is well, and the calibration strategy solves the influence of the initial parameters on the estimation accuracy. The experimental results of the improved IFFRLS-ASRUKF show that the SOC estimation accuracy is high, which meets the practical requirements of the vehicle-level battery pack.

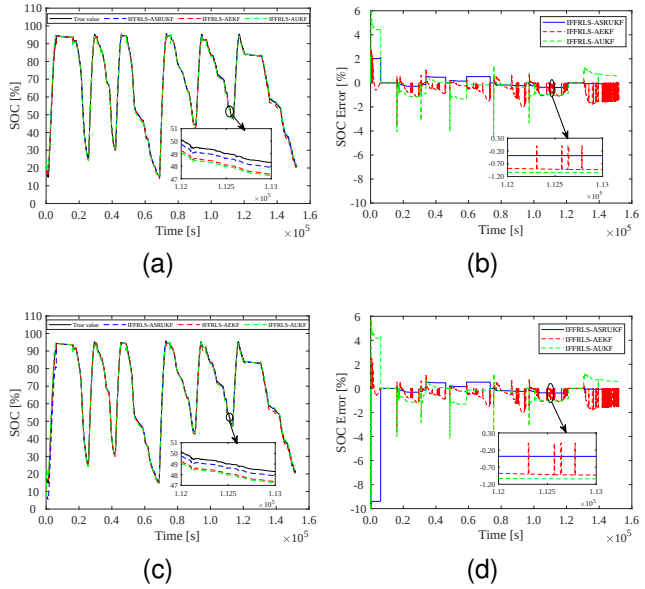

Fig. 13. Comparison between vehicle-level simulated results and real data of the battery pack. (a) SOC estimation with known initial SOC. (b) SOC estimation error with known initial SOC. (c) SOC estimation with unknown initial SOC. (d) SOC estimation error with unknown initial SOC.

TABLE IV
PERFORMANCE COMPARISON OF IFFRLS-BASED ADAPTIVE SOC ESTIMATION METHODS UNDER REAL-WORLD OPERATING CONDITIONS.

Method	Max. Err.	MAE	RMSE
ASRUKF	2.15%	0.22%	0.47%
AEKF	3.74%	0.58%	0.88%
AUKF	4.92%	0.42%	0.79%

V. CONCLUSIONS

This paper proposes a model-based battery pack SOC estimation framework to solve the numerical problems in conventional BMS. The main conclusions are as follows.

1) The first-order RC ECM model parameters are identified online by combining the time window with FFRLS. An adaptive algorithm is proposed to adapt the forgetting factor with the voltage prediction error. In addition, the sliding time window avoids abnormal data caused by inaccurate parameter identification and improves the algorithm's stability.

2) A strategy is proposed that includes full charge correction, static calibration, and operating state discrimination. With the calibration strategy, the influence of the initial parameters on the estimation accuracy is mitigated. As a result, it improves the estimation accuracy and stability of the whole estimation algorithm.

3) The improved IFFRLS-ASRUKF algorithm is verified under cell tests and real-world driving conditions with a large-size battery pack. This algorithm's maximum SOC error and RMSE can be controlled within 1% and 0.47%, respectively. The results meet the practical requirements of vehicle-level SOC estimation for EVs.

The SOC estimation and cell screening strategy adopted in this paper cannot fully represent the performance of the battery pack under the premise of ensuring the safety of the battery pack, and there will be a certain loss of accuracy. In future research, the estimation accuracy of battery pack SOC should be further improved by establishing more accurate battery modeling with the consideration of dynamics related to cell inconsistency, aging, and safety. In addition, it is necessary to explore accurate SOC estimation algorithms for battery packs over the entire life cycle and under all possible operating conditions, such as full temperature ranges.

ACKNOWLEDGMENTS

The authors would like to thank Changfu Zou from Chalmers University of Technology for useful discussions and proofreading of the manuscript.

REFERENCES

[1] H. Wang, H. Liu, J. Yao, D. Ye, Z. Lang, and A. Glowacz, "Mapping the knowledge domains of new energy vehicle safety: Informetrics analysis-based studies," *J. Energy Storage*, vol. 35, p. 102275, 2021.

[2] M. Hossain Lipu, M. Hannan, A. Hussain, A. Ayob, M. H. Saad, T. F. Karim, and D. N. How, "Data-driven state of charge estimation of lithium-ion batteries: Algorithms, implementation factors, limitations and future trends," *J. Cleaner Prod.*, vol. 277, p. 124110, 2020.

[3] X. Hu, H. Yuan, C. Zou, Z. Li, and L. Zhang, "Co-estimation of state of charge and state of health for lithium-ion batteries based on fractional-order calculus," *IEEE Transactions on Vehicular Technology*, vol. 67, no. 11, pp. 10 319–10 329, 2018.

[4] K. Liu, Y. Gao, C. Zhu, K. Li, M. Fei, C. Peng, X. Zhang, and Q.-L. Han, "Electrochemical modeling and parameterization towards control-oriented management of lithium-ion batteries," *Control Eng. Practice*, vol. 124, p. 105176, 2022.

[5] Y. Li, T. Wik, C. Xie, Y. Huang, B. Xiong, J. Tang, and C. Zou, "Control-oriented modeling of all-solid-state batteries using physics-based equivalent circuits," *IEEE Trans. Transport. Electrific.*, vol. 8, no. 2, pp. 2080–2092, Aug. 2022.

[6] A. Mondal, A. Routray, and S. Puravankara, "Parameter identification and co-estimation of state-of-charge of li-ion battery in real-time on internet-of-things platform," *J. Energy Storage*, vol. 51, p. 104370, 2022.

[7] X. Dang, L. Yan, K. Xu, X. Wu, H. Jiang, and H. Sun, "Open-circuit voltage-based state of charge estimation of lithium-ion battery using dual neural network fusion battery model," *Electrochim. Acta*, vol. 188, pp. 356–366, 2016.

[8] Y. Li, D. Karunathilake, D. M. Vilathgamuwa, Y. Mishra, T. W. Farrell, S. S. Choi, and C. Zou, "Model order reduction techniques for physics-based lithium-ion battery management: A survey," *IEEE Ind. Electron. Mag.*, vol. 16, no. 3, pp. 36–51, 2022.

[9] C. She, Y. Li, C. Zou, T. Wik, Z. Wang, and F. Sun, "Offline and online blended machine learning for lithium-ion battery health state estimation," *IEEE Trans. Transport. Electrific.*, vol. 8, no. 2, pp. 1604–1618, Aug. 2022.

[10] A. V. Vykhodtsev, D. Jang, Q. Wang, W. Rosehart, and H. Zareipour, "A review of modelling approaches to characterize lithium-ion battery energy storage systems in techno-economic analyses of power systems," *Renew. Sustain. Energy Rev.*, vol. 166, p. 112584, 2022.

[11] J. Tian, R. Xiong, W. Shen, J. Wang, and R. Yang, "Online simultaneous identification of parameters and order of a fractional order battery model," *J. Cleaner Prod.*, vol. 247, p. 119147, 2020.

[12] M.-K. Tran, M. Mathew, S. Janhunen, S. Panchal, K. Raahemifar, R. Fraser, and M. Fowler, "A comprehensive equivalent circuit model for lithium-ion batteries, incorporating the effects of state of health, state of charge, and temperature on model parameters," *J. Energy Storage*, vol. 43, p. 103252, 2021.

[13] K. Mc Carthy, H. Gullapalli, K. M. Ryan, and T. Kennedy, "Electrochemical impedance correlation analysis for the estimation of li-ion battery state of charge, state of health and internal temperature," *J. Energy Storage*, vol. 50, p. 104608, 2022.

[14] Z. Wang, G. Feng, X. Liu, F. Gu, and A. Ball, "A novel method of parameter identification and state of charge estimation for lithium-ion battery energy storage system," *J. Energy Storage*, vol. 49, p. 104124, 2022.

[15] J. Wu, C. Fang, Z. Jin, L. Zhang, and J. Xing, "A multi-scale fractional-order dual unscented kalman filter based parameter and state of charge joint estimation method of lithium-ion battery," *J. Energy Storage*, vol. 50, p. 104666, 2022.
[16] M. Hossain, M. Haque, and M. Arif, "Kalman filtering techniques for the online model parameters and state of charge estimation of the li-ion batteries: A comparative analysis," *J. Energy Storage*, vol. 51, p. 104174, 2022.
[17] I. Jarrraya, L. Degaa, N. Rizoug, M. H. Chabchoub, and H. Trabelsi, "Comparison study between hybrid nelder-mead particle swarm optimization and open circuit voltage recursive least square for the battery parameters estimation," *J. Energy Storage*, vol. 50, p. 104424, 2022.
[18] X. Lai, Y. Huang, H. Gu, X. Han, X. Feng, H. Dai, Y. Zheng, and M. Ouyang, "Remaining discharge energy estimation for lithium-ion batteries based on future load prediction considering temperature and ageing effects," *Energy*, vol. 238, p. 121754, 2022.
[19] M. Wu, L. Qin, and G. Wu, "State of charge estimation of power lithium-ion battery based on an affine iterative adaptive extended kalman filter," *J. Energy Storage*, vol. 51, p. 104472, 2022.
[20] X. Lai, L. He, S. Wang, L. Zhou, Y. Zhang, T. Sun, and Y. Zheng, "Co-estimation of state of charge and state of power for lithium-ion batteries based on fractional variable-order model," *J. Cleaner Prod.*, vol. 255, p. 120203, 2020.
[21] N. Mohammed and A. M. Saif, "Programmable logic controller based lithium-ion battery management system for accurate state of charge estimation," *Computers & Electrical Engineering*, vol. 93, p. 107306, 2021.
[22] C. Jiang, S. Wang, B. Wu, C. Fernandez, X. Xiong, and J. Coffie-Ken, "A state-of-charge estimation method of the power lithium-ion battery in complex conditions based on adaptive square root extended kalman filter," *Energy*, vol. 219, p. 119603, 2021.
[23] T. Zahid, K. Xu, W. Li, C. Li, and H. Li, "State of charge estimation for electric vehicle power battery using advanced machine learning algorithm under diversified drive cycles," *Energy*, vol. 162, pp. 871–882, 2018.
[24] S. Wang, P. Takyi-Aninakwa, S. Jin, C. Yu, C. Fernandez, and D.-I. Stroe, "An improved feedforward-long short-term memory modeling method for the whole-life-cycle state of charge prediction of lithium-ion batteries considering current-voltage-temperature variation," *Energy*, vol. 254, p. 124224, 2022.
[25] C. Bian, S. Yang, and Q. Miao, "Cross-domain state-of-charge estimation of li-ion batteries based on deep transfer neural network with multiscale distribution adaptation," *IEEE Trans. Transport. Electrific.*, vol. 7, no. 3, pp. 1260–1270, 2021.
[26] Z. Deng, X. Hu, X. Lin, Y. Che, L. Xu, and W. Guo, "Data-driven state of charge estimation for lithium-ion battery packs based on gaussian process regression," *Energy*, vol. 205, p. 118000, 2020.
[27] Q. Wang, M. Ye, M. Wei, G. Lian, and C. Wu, "Co-estimation of state of charge and capacity for lithium-ion battery based on recurrent neural network and support vector machine," *Energy Rep.*, vol. 7, pp. 7323–7332, 2021.
[28] I.-S. Kim, "The novel state of charge estimation method for lithium battery using sliding mode observer," *Journal of Power Sources*, vol. 163, no. 1, pp. 584–590, 2006.
[29] C. Xu, E. Zhang, S. Yan, K. Jiang, K. Wang, Z. Wang, and S. Cheng, "State of charge estimation for liquid metal battery based on an improved sliding mode observer," *Journal of Energy Storage*, vol. 45, p. 103701, 2022.
[30] Z. Chen, J. Zhou, F. Zhou, and S. Xu, "State-of-charge estimation of lithium-ion batteries based on improved h infinity filter algorithm and its novel equalization method," *J. Cleaner Prod.*, vol. 290, p. 125180, 2021.
[31] M. Hannan, M. Lipu, A. Hussain, and A. Mohamed, "A review of lithium-ion battery state of charge estimation and management system in electric vehicle applications: Challenges and recommendations," *Renew. Sustain. Energy Rev.*, vol. 78, pp. 834–854, 2017.
[32] J. Xie, J. Ma, and J. Chen, "Available power prediction limited by multiple constraints for lifepo4 batteries based on central difference kalman filter," *Int. J. Energy Res.*, vol. 42, no. 15, pp. 4730–4745, 2018.
[33] V. Basetti, A. K. Chandel, and C. K. Shiva, "Square-root cubature kalman filter based power system dynamic state estimation," *Sustain. Energy Grids Netw.*, vol. 31, p. 100712, 2022.
[34] X. Shu, G. Li, Y. Zhang, S. Shen, Z. Chen, and Y. Liu, "Stage of charge estimation of lithium-ion battery packs based on improved cubature kalman filter with long short-term memory model," *IEEE Trans. Transport. Electrific.*, vol. 7, no. 3, pp. 1271–1284, 2021.
[35] L. Ma, Y. Xu, H. Zhang, F. Yang, X. Wang, and C. Li, "Co-estimation of state of charge and state of health for lithium-ion batteries based on fractional-order model with multi-innovations unscented kalman filter method," *J. Energy Storage*, vol. 52, p. 104904, 2022.
[36] Y. Li, B. Xiong, D. M. Vilathgamuwa, Z. Wei, C. Xie, and C. Zou, "Constrained ensemble kalman filter for distributed electrochemical state estimation of lithium-ion batteries," *IEEE Trans. Ind. Informat.*, vol. 17, no. 1, pp. 240–250, Jan. 2021.
[37] R. Zhu, B. Duan, J. Zhang, Q. Zhang, and C. Zhang, "Co-estimation of model parameters and state-of-charge for lithium-ion batteries with recursive restricted total least squares and unscented kalman filter," *Appl. Energy*, vol. 277, p. 115494, 2020.
[38] L. Chen, X. Wu, A. M. Lopes, L. Yin, and P. Li, "Adaptive state-of-charge estimation of lithium-ion batteries based on square-root unscented kalman filter," *Energy*, vol. 252, p. 123972, 2022.
[39] Y. Li, C. Wang, and J. Gong, "A multi-model probability soc fusion estimation approach using an improved adaptive unscented kalman filter technique," *Energy*, vol. 141, pp. 1402–1415, 2017.
[40] C. Liu, M. Hu, G. Jin, Y. Xu, and J. Zhai, "State of power estimation of lithium-ion battery based on fractional-order equivalent circuit model," *J. Energy Storage*, vol. 41, p. 102954, 2021.
[41] L. Hu, X. Hu, Y. Che, F. Feng, X. Lin, and Z. Zhang, "Reliable state of charge estimation of battery packs using fuzzy adaptive federated filtering," *Appl. Energy*, vol. 262, p. 114569, 2020.
[42] X. Liu, K. Li, J. Wu, Y. He, and X. Liu, "An extended kalman filter based data-driven method for state of charge estimation of li-ion batteries," *J. Energy Storage*, vol. 40, p. 102655, 2021.
[43] D. Wang, X. Li, J. Wang, Q. Zhang, B. Yang, and Z. Hao, "Lithium-ion battery equivalent model over full-range state of charge based on electrochemical process simplification," *Electrochim. Acta*, vol. 389, p. 138698, 2021.
[44] C. Ge, Y. Zheng, and Y. Yu, "State of charge estimation of lithium-ion battery based on improved forgetting factor recursive least squares-extended kalman filter joint algorithm," *J. Energy Storage*, vol. 55, p. 105474, 2022.
[45] R. Mohammadi Asl, Y. Shabbouei Hagh, S. Simani, and H. Handroos, "Adaptive square-root unscented kalman filter: An experimental study of hydraulic actuator state estimation," *Mechan. Syst. Signal Processing*, vol. 132, pp. 670–691, 2019.
[46] Z. Shuzhi, G. Xu, and Z. Xiongwen, "A novel one-way transmitted co-estimation framework for capacity and state-of-charge of lithium-ion battery based on double adaptive extended kalman filters," *J. Energy Storage*, vol. 33, p. 102093, 2021.
[47] J. Yuan, Y. Wang, and Z. Ji, "A differentially private square root unscented kalman filter for protecting process parameters in icpss," *ISA Trans.*, vol. 104, pp. 44–52, 2020.
[48] H. Ramazan, "Adaptive robust unscented kalman filter with recursive least square for state of charge estimation of batteries," *Electr. Eng.*, vol. 104, pp. 1001–1017, 2022.
[49] C. Sun, H. Lin, H. Cai, M. Gao, C. Zhu, and Z. He, "Improved parameter identification and state-of-charge estimation for lithium-ion battery with fixed memory recursive least squares and sigma-point kalman filter," *Electrochim. Acta*, vol. 387, p. 138501, 2021.
[50] J. Hou, J. Liu, F. Chen, P. Li, T. Zhang, J. Jiang, and X. Chen, "Robust lithium-ion state-of-charge and battery parameters joint estimation based on an enhanced adaptive unscented kalman filter," *Energy*, vol. 271, p. 126998, 2023.

Xiaohua Wu received the B.S. degree from the College of Engineering, China Agricultural University, Beijing, China, in 2007, and the Ph.D. degree in Automotive Engineering from the Beijing Institute of Technology, Beijing, in 2011. She is currently a Professor with the School of Automobile and Transportation, Xihua University, Chengdu, China, and a Visiting Scholar with Chalmers University of Technology, Gothenburg, Sweden. She was a Visiting Scholar at the University of California, Berkeley, USA, from 2014 to 2015. Her research interests include data-driven and electrochemical mechanism modeling, parameter identification, state estimation of lithium-ion batteries and proton exchange membrane fuel cells, and optimal energy management strategy of hybrid energy systems.

Zhanfeng Fan received his B.S. and M.S. degrees from the Chengdu University of Technology, Chengdu, China, in 2007 and 2010, respectively, and received the Ph.D. degree from Southwest Jiaotong University, Chengdu, China, in 2020. He is a Lecturer at the School of Architecture and Civil Engineering, Chengdu University, China. His research interests focus on the numerical simulation of multi-physical field coupling, life prediction of battery and proton exchange membrane fuel cells, and porous media fluid mechanics calculation.

Jianbo Xie received the B.S. degree in Automotive Engineering from Xihua University in Chengdu, China, in 2015. He is currently a Senior Manager for system development at WM Motor Technology Co, Ltd. He works in the fields of technology solutions for battery management units and charging systems.

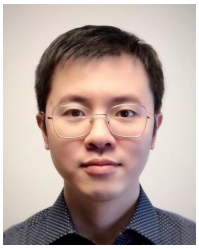

Yang Li (Senior Member, IEEE) received the B.E. degree in electrical engineering from Wuhan University, Wuhan, China, in 2007, and the M.Sc. and Ph.D. degrees in power engineering from Nanyang Technological University (NTU), Singapore, in 2008 and 2015, respectively. He was a Research Fellow with the Energy Research Institute, NTU and the School of Electrical Engineering and Computer Science, Queensland University of Technology, Brisbane, QLD, Australia. He joined the School of Automation, Wuhan University of Technology, Wuhan, in 2019, as a faculty member. Since 2020, he has been a Researcher with the Department of Electrical Engineering, Chalmers University of Technology, Gothenburg, Sweden. His research interests include modeling and control of energy storage systems in power grid and transport sectors.

Dr. Li is a recipient of the EU Marie Skłodowska-Curie Action Individual Fellowship in 2020. He serves as an Associate Editor for several IEEE journals, such as IEEE TRANSACTIONS ON ENERGY CONVERSION, IEEE TRANSACTIONS ON INDUSTRIAL ELECTRONICS, and IEEE TRANSACTIONS ON TRANSPORTATION ELECTRIFICATION.

Junhao Shu received the B.S. degree in Automotive Engineering from Xihua University in Chengdu, China, in 2020, where he is pursuing an M.S. degree with a focus on the parameter identification and state estimation of lithium-ion batteries.

Jibin Yang received the B.S. degree in automation from Lanzhou Jiaotong University in 2011, and the M.S. and Ph.D. degrees in vehicle operation engineering from Southwest Jiaotong University, Chengdu, China, in 2013 and 2018, respectively. He is currently an Associate Professor at the School of Automobile and Transportation, Xihua University, Chengdu. His research interests include optimal control, sizing and energy management strategy of hybrid system for hybrid vehicles.

Zhongwei Deng (Member, IEEE) received his Ph.D. in Mechanical Engineering from Shanghai Jiao Tong University, Shanghai, China, in 2019. He previously finished his B.S. from Jilin University, China, in 2014. He was a Postdoctoral Researcher in the College of Mechanical and Vehicle Engineering, Chongqing University. He is currently an Associate Professor at the School of Mechanical and Electrical Engineering, University of Electronic Science and Technology of China. His research interests focus on data-driven and electrochemical mechanism modeling, parameter identification, state estimation, health diagnosis, and second-life utilization of lithium-ion batteries.